Numerical Investigation of Electromagnetic Wave Propagation Phenomena by Three-Dimensional Meshless Time-Domain Method*)

Yoshiharu OHI and Soichiro IKUNO[1)]

RIKEN Advanced Institute for Computational Science, 7-1-26 Minatojima-minami-machi, Chuo-ku, Kobe, Hyogo 650-0047, Japan

[1)]*Tokyo University of Technology, 1404-1 Katakura-machi, Hachioji, Tokyo 192-0982, Japan*

(Received 25 November 2014 / Accepted 9 March 2015)

The finite-difference time-domain method (FDTDM) is commonly applied to time dependent electromagnetic wave propagation simulations. In the FDTDM, the nodes of electric and magnetic fields are located based on an orthogonal mesh called the Yee-lattice. However, using this method, it is difficult to express a complex shaped domain. The radial point interpolation method (RPIM) is a meshless method that can be applied to electromagnetic wave propagation simulations. The meshless time-domain method (MTDM) based on RPIM can treat complex shaped domains easily. In previous studies, the computational accuracy and numerical stability of the three-dimensional (3-D) MTDM has not been clear. The present study numerically investigates the influence of weight functions on the computational accuracy and numerical stability of the 3-D MTDM. We perform numerical simulations, the results of which show that the multi-quadratic, reciprocal multi-quadratic and quadratic spline functions should be employed for the weight functions.

Keywords: finite-difference time-domain method, meshless time-domain method, radial point interpolation method

DOI: 10.1585/pfr.10.3406072

1. Introduction

The finite-difference time-domain method (FDTDM) is widely used for numerical simulations of electromagnetic wave propagation phenomena. The governing equations of the FDTDM are discretized by using the leapfrog and central difference methods [1]. The nodes of the electric and magnetic fields are located based on an orthogonal mesh called the Yee-lattice. FDTDM has a great advantage with respect to discretization, but cannot easily express a complex shaped domain.

Recently, various meshless methods such as the radial point interpolation method (RPIM) have been proposed [2, 3]. The meshless time-domain method (MTDM) based on RPIM can be applied to electromagnetic wave propagation simulations [4–6]. In the MTDM, the governing equations are discretized using the leapfrog method, a shape function and a partial derivative of the shape function. The nodes of the electric and magnetic fields can be located without requiring a mesh. Therefore, it is easy to express a complex shaped domain. However, the influence of weight functions on the computational accuracy and numerical stability has not been clarified in the three-dimensional (3-D) MTDM in previous studies. The purpose of the present study is to numerically investigate the influence of weight functions on the computational accuracy and numerical stability of the 3-D MTDM.

2. Meshless Time-Domain Method

In the MTDM, a shape function and a partial derivative of the shape function are derived, based on the RPIM, which is a meshless method. In the RPIM, nodes are scattered at arbitrary positions in the analysis domain Ω, as shown in Fig. 1. An approximation function $u^*(\boldsymbol{x})$ and a partial derivative of the approximation function $\partial u^*(\boldsymbol{x})$ are expanded as follows using a shape function $\boldsymbol{\phi}(\boldsymbol{x})$, a partial derivative of the shape function $\partial\boldsymbol{\phi}(\boldsymbol{x})$ and a known vector $\boldsymbol{u}$:

$$u^*(\boldsymbol{x}) = (\boldsymbol{\phi}(\boldsymbol{x}), \boldsymbol{u}) = \sum_i \phi_i(\boldsymbol{x}) u_i, \tag{1}$$

$$\partial u^*(\boldsymbol{x}) = (\partial\boldsymbol{\phi}(\boldsymbol{x}), \boldsymbol{u}) = \sum_i \partial\phi_i(\boldsymbol{x}) u_i, \tag{2}$$

where $\boldsymbol{x}$ is the position vector and $(\boldsymbol{a}, \boldsymbol{b})$ denotes an inner product of the vectors $\boldsymbol{a}$ and $\boldsymbol{b}$. ∂ means $\partial/\partial x$, $\partial/\partial y$ and $\partial/\partial z$ in the 3-D case. The domain of influence is defined by a parameter R, called the "support radius". Nodes in the domain of influence (the open circles within the circle of radius R in Fig. 1) contribute to the value of the approximation function at the point $\boldsymbol{x}$. A shape function and a partial derivative of the shape function are generated by solving a system of linear equations as:

author's e-mail: yoshiharu.ohi@riken.jp

*) This article is based on the presentation at the 24th International Toki Conference (ITC24).

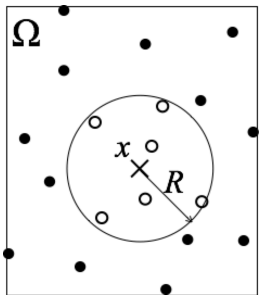

Fig. 1 Conceptual diagram of node distribution and domain of influence in the radial point interpolation method.

$$G(\boldsymbol{x})\left[\frac{\boldsymbol{\phi}(\boldsymbol{x})}{\boldsymbol{X}(\boldsymbol{x})}\right]=\left[\frac{\boldsymbol{b}^*(\boldsymbol{x})}{\boldsymbol{p}^*(\boldsymbol{x})}\right], \tag{3}$$

$$G(\boldsymbol{x})\left[\frac{\partial\boldsymbol{\phi}(\boldsymbol{x})}{\boldsymbol{X}(\boldsymbol{x})}\right]=\left[\frac{\partial\boldsymbol{b}^*(\boldsymbol{x})}{\partial\boldsymbol{p}^*(\boldsymbol{x})}\right], \tag{4}$$

where $G(\boldsymbol{x})$ is a coefficient matrix, $\boldsymbol{X}(\boldsymbol{x})$ is an unknown vector and $\boldsymbol{b}^*(\boldsymbol{x})$ and $\boldsymbol{p}^*(\boldsymbol{x})$ are known vectors. $\boldsymbol{b}^*(\boldsymbol{x})$ and $\boldsymbol{p}^*(\boldsymbol{x})$ are generated by the radial basis function (RBF) and the polynomial basis function (PBF). The coefficient matrix $G(\boldsymbol{x})$ consists of sub matrices as:

$$G=\left[\begin{array}{c|c} B_0 & P_0 \\ \hline P_0^{\mathrm{T}} & O \end{array}\right], \tag{5}$$

where B_0 and P_0 are also generated by the RBF and PBF, and P_0^{T} is the transverse of P_0. In the 3-D case, PBF is defined as $\boldsymbol{p}(\boldsymbol{x}) = [1, x, y, z]$. The RBF, $b(r)$, is defined as a function of the distance r between a point $\boldsymbol{x}$ and nodes in the domain of influence $\boldsymbol{x}_i$ ($r = |\boldsymbol{x} - \boldsymbol{x}_i|$) [7] [8]. Here, the computational accuracy and numerical stability depend on the type of RBF and the support radius R. In the present study, four types of RBF are employed for numerical investigations, defined by equations (6)–(8) below. Equation (6) with $s = 0.5$ is called the "multi-quadratic (MQ)", and with $s = -0.5$ it is called the "reciprocal multi-quadratic (RMQ)". Equations (7) and (8) are the "exponential weight function (EWF)" and "the quadratic spline function (QSF)". c is called the "support coefficient", and is fixed at 1.0 in the present study. RBF of all types satisfy equation (9).

$$b(r)=\left(\left(\frac{r}{R}\right)^2+1.0\right)^s, \tag{6}$$

$$b(r)=\frac{\mathrm{e}^{-(r/c)^2}-\mathrm{e}^{-(R/c)^2}}{1.0-\mathrm{e}^{-(R/c)^2}}, \tag{7}$$

$$b(r)=1.0-6.0\left(\frac{r}{R}\right)^2+8.0\left(\frac{r}{R}\right)^3-3.0\left(\frac{r}{R}\right)^4, \tag{8}$$

$$b(r)=0: \quad r\geq R. \tag{9}$$

The shape function based on the RPIM satisfies the delta function property as:

$$\phi_i(\boldsymbol{x}=\boldsymbol{x}_j)=\begin{cases} 1, & i=j, \\ 0, & i\neq j. \end{cases} \tag{10}$$

From this, an approximation function can be described in a simplified form:

$$u^*(\boldsymbol{x}_i)=(\boldsymbol{\phi}(\boldsymbol{x}_i),\boldsymbol{u})=u_i. \tag{11}$$

This property is very important for the discretization and approximation of the governing equations.

The Maxwell equations, which are the governing equation of MTDM, are discretized and approximated. The Maxwell equations are written as:

$$\varepsilon\frac{\partial\boldsymbol{E}}{\partial t}=-\sigma\boldsymbol{E}+\nabla\times\boldsymbol{H}, \tag{12}$$

$$\mu\frac{\partial\boldsymbol{H}}{\partial t}=-\nabla\times\boldsymbol{E}, \tag{13}$$

where $\boldsymbol{E}$ and $\boldsymbol{H}$ are the electric and magnetic fields, ε, μ and σ are the electric permittivity, magnetic permeability and electrical conductivity, respectively. Equations (12) and (13) can be discretized with respect to time and space by using the leapfrog method, a shape function and a partial derivative of the shape function, giving:

$$E_{x,i}^{n+1}=C_E E_{x,i}^n +C_{EH}\left(\sum_j\frac{\partial\phi_{i,j}^{H_z}}{\partial y}H_{z,j}^{n+\frac{1}{2}}-\sum_k\frac{\partial\phi_{i,k}^{H_y}}{\partial z}H_{y,k}^{n+\frac{1}{2}}\right), \tag{14}$$

$$E_{y,i}^{n+1}=C_E E_{y,i}^n +C_{EH}\left(\sum_j\frac{\partial\phi_{i,j}^{H_x}}{\partial z}H_{x,j}^{n+\frac{1}{2}}-\sum_k\frac{\partial\phi_{i,k}^{H_z}}{\partial x}H_{z,k}^{n+\frac{1}{2}}\right), \tag{15}$$

$$E_{z,i}^{n+1}=C_E E_{z,i}^n +C_{EH}\left(\sum_j\frac{\partial\phi_{i,j}^{H_y}}{\partial x}H_{y,j}^{n+\frac{1}{2}}-\sum_k\frac{\partial\phi_{i,k}^{H_x}}{\partial y}H_{x,k}^{n+\frac{1}{2}}\right), \tag{16}$$

$$H_{x,i}^{n+\frac{1}{2}}=H_{x,i}^{n-\frac{1}{2}} +\frac{\Delta t}{\mu}\left(\sum_j\frac{\partial\phi_{i,j}^{E_y}}{\partial z}E_{y,j}^n-\sum_k\frac{\partial\phi_{i,k}^{E_z}}{\partial y}E_{z,k}^n\right), \tag{17}$$

$$H_{y,i}^{n+\frac{1}{2}}=H_{y,i}^{n-\frac{1}{2}} +\frac{\Delta t}{\mu}\left(\sum_j\frac{\partial\phi_{i,j}^{E_z}}{\partial x}E_{z,j}^n-\sum_k\frac{\partial\phi_{i,k}^{E_x}}{\partial z}E_{x,k}^n\right), \tag{18}$$

$$H_{z,i}^{n+\frac{1}{2}}=H_{z,i}^{n-\frac{1}{2}} +\frac{\Delta t}{\mu}\left(\sum_j\frac{\partial\phi_{i,j}^{E_x}}{\partial y}E_{x,j}^n-\sum_k\frac{\partial\phi_{i,k}^{E_y}}{\partial x}E_{y,k}^n\right), \tag{19}$$

$$C_E=\left(1-\frac{\sigma\Delta t}{2\varepsilon}\right)/\left(1+\frac{\sigma\Delta t}{2\varepsilon}\right), \tag{20}$$

$$C_{EH}=\left(\frac{\Delta t}{\varepsilon}\right)/\left(1+\frac{\sigma\Delta t}{2\varepsilon}\right), \tag{21}$$

where n is the time step. E_x, E_y, E_z, H_x H_y and H_z are the x-, y- and z-components of the electric and magnetic fields, and $\partial\phi^H$ and $\partial\phi^E$ are the partial derivatives of the shape functions for the magnetic and electric fields, respectively. A vacuum region ($\sigma = 0$) is employed in the

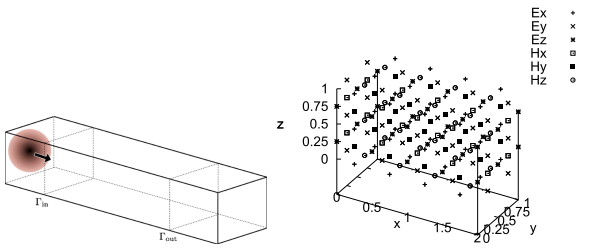

Fig. 2 Conceptual diagram of waveguide (a) and node distribution based on a 3-D staggered mesh (b).

Table 1 Physical parameters for the waveguide and input wave.

Size of waveguide	10 [m] × 1 [m] × 1 [m]
Distance between nodes	5 [cm]
Source wave form	Sine wave
Frequency of source	6.0×10^8 [Hz]

analysis domain in the numerical evaluation of the present study and thus equations (20) and (21) become $C_E = 1$ and $C_{EH} = \Delta t/\varepsilon$. A time dependent solution is given by solving equations (14)–(21) while updating the time step n.

3. Numerical Evaluation

Previous studies have investigated the influence of the weight functions or node arrangement on the computational accuracy and numerical stability in two-dimensional MTDM [9]. In the present study, in order to investigate the influence of the weight functions on the computational accuracy and numerical stability of the 3-D MTDM, simulations are performed using a straight waveguide as shown in Fig. 2 (a). For simplicity, the nodes of the electric and magnetic fields are arranged based on a staggered mesh as shown in Fig. 2 (b). A perfect electric conductor is employed as the wall of the waveguide so that the perpendicular component of the electric field is set to zero at the wall as the Dirichlet boundary condition. The source of the electromagnetic wave is input at the edge of the waveguide. The other physical parameters are summarized in Table 1. The Poynting vector [10] is measured on the surfaces at Γ_{in} and Γ_{out}, and the transmission rate T_{R} is defined as:

$$T_{\text{R}} = \frac{\langle P \rangle_{\Gamma_{\text{out}}}}{\langle P \rangle_{\Gamma_{\text{in}}}}, \tag{22}$$

$$\langle P \rangle = \frac{\int_T \int_\Gamma P \mathrm{d}S \, \mathrm{d}t}{T}, \tag{23}$$

where T and P are the period of the source wave and Poynting vector, and $\int_\Gamma \mathrm{d}S$ and $\frac{1}{T}\int_T \mathrm{d}t$ denote the surface integration and the average of time, respectively. In the present study, it is considered that the computational accuracy is good if T_{R} is near to 1.0.

The transmission rates T_{R} for the support radius R and RBF are summarized in Table 2. If the EWF is employed for the RBF, the calculations failed for all R and hence the results for EWF are not listed in Table 2. It can be seen that the MQ, RMQ or QSF can be employed for the RBF. Some values of T_{R} are over 1.0, representing reflections from the wall. In addition, we found that numerical unevenness is caused by variation of the number of nodes in the domain of influence. In order to investigate the influence of the number of nodes in the domain of influence on the computational accuracy, we measured the transmission rates T_{R} for N_{min}, where N_{min} is the minimum number of nodes in the domain of influence.

Table 2 Transmission rates T_{R} for support radius R and RBF.

R [cm]	MQ	RMQ	QSF
7.5	0.96220	0.96838	0.89398
10.0	1.01445	1.02405	1.00680
12.5	1.00129	1.01970	0.99985

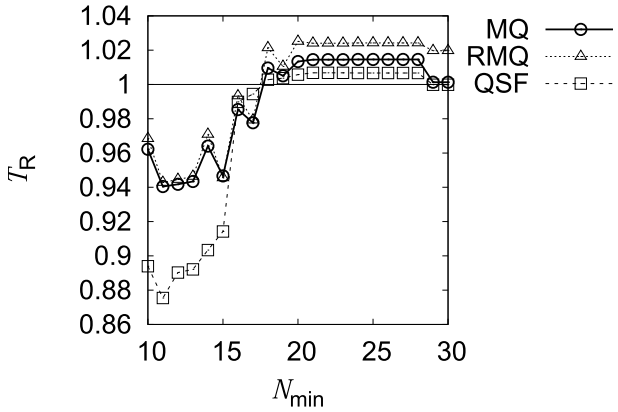

Fig. 3 Transmission rates T_{R} for N_{min} plotted using MQ, RMQ and QSF.

Fig. 3 shows the transmission rates T_{R} for N_{min}. The calculations failed if N_{min} is less than 10. Specifically, if N_{min} is less than 10, the generation process of partial derivatives of the shape functions failed. This contrasts with our expectation that calculation should be possible if N is more than 4. In addition, N_{min} should be set to be more than 16 for stable computation. Furthermore, the computational accuracy is not improved necessarily if N_{min} increases. The reasons for these results are not currently clear and a detailed mathematical analysis is necessary.

A stability condition for the time step is necessary because the Maxwell equations are hyperbolic partial differential equations and the leapfrog method is an explicit method. The stability condition for the time step in MTDM is written as:

$$\Delta t < \frac{\min |\boldsymbol{x}_i - \boldsymbol{x}_j|}{C}, \tag{24}$$

where C is the velocity of light and $\boldsymbol{x}_i$ and $\boldsymbol{x}_j$ are the positions of the nodes of the electric or magnetic field [6]. In order to investigate the influence of the time step on the numerical stability, we measured the transmission rates T_{R}

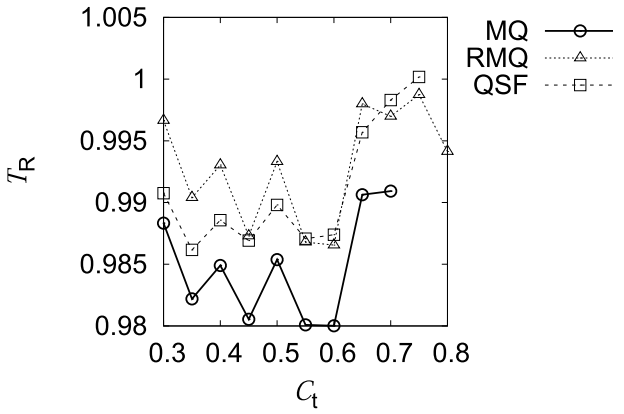

Fig. 4 Transmission rates T_R for C_t plotted using MQ, RMQ and QSF.

for Δt. For the evaluation, Δt is set as:

$$\Delta t = C_t \frac{\min |\boldsymbol{x}_i - \boldsymbol{x}_j|}{C}, \tag{25}$$

where C_t is the stability coefficient. The transmission rate T_R for C_t was measured using the MQ, RMQ and QSF for $N_{min} = 16$, and is plotted in Fig. 4. We can see from this result that T_R using each RBF shows similar behavior. C_t should be set to be less than 0.8, lower than the theoretical value. The computational accuracy does not improve even if C_t becomes small. The reason for this result is not currently clear and further detailed mathematical analysis is required.

4. Conclusion

In the present study, the influence of the weight functions on the computational accuracy and numerical stability of the 3-D MTDM is investigated numerically. The conclusions obtained in the present study are summarized as follows.

- The multi-quadratic, reciprocal multi-quadratic or quadratic spline functions should be employed for the radial basis function.
- At least 10 nodes in the domain of influence are necessary for a stable calculation.
- The support radius R should be decided in consideration of the number of nodes in the domain of influence.
- The computational accuracy does not necessarily improve if the minimum number of nodes in the domain of influence increases and the time step becomes small.
- The time step Δt should be set to be lower than the theoretical value.

Some difficult problems for stable computation using MTDM are still unclear, such as, the relation between the number of nodes in the domain of influence and the computational accuracy, and the relation between the time step and numerical stability. To clarify these problems, a detailed mathematical analysis is necessary, and is planned as a future study.

[1] K.S. Yee, IEEE Trans. Antennas Propag. **14**, 3, 302 (1966).
[2] T. Belytschko, L.Y. Yun and T. Lei, Int. J. Numer. Methods Eng. **37**, 2, 229 (1994).
[3] J.G. Wang and G.R. Liu, Int. J. Numer. Methods Eng. **54**, 11, 1623 (2002).
[4] T. Kaufmann, F. Christophe and V. Rudiger, Microwave Symposium Digest, 2008 IEEE MTT-S International, pp.61-64.
[5] T. Kaufmann, C. Engstrom, C. Fumeaux and R. Vahldieck, IEEE Trans. Microw. Theory Tech. **58**, 12, 3399 (2010).
[6] S. Ikuno, Y. Fujita, Y. Hirokawa, T. Itoh, S. Nakata and A. Kamitani, IEEE Trans. Magn. **49**, 5, 1613 (2013).
[7] M. Powell, *The Theory of Radial Basis Function Approximation in 1990* (Oxford, 1992) pp.105-203.
[8] G.E. Fasshauer, Proceedings of Chamonix, Vanderbilt University Press Nashville, TN, 1997 (1996), pp.1-8.
[9] Y. Ohi, Y. Fujita, T. Itoh, H. Nakamura and S. Ikuno, Plasma Fusion Res. **9**, 3401144 (2014).
[10] R. Becker and F. Sauter, *Electromagnetic Fields and Interactions* (Dover Publications, New York, 1982).